Orbital eccentricities in primordial black hole binaries

Ilias Cholis,[*] Ely D. Kovetz,[†] Yacine Ali-Haïmoud,[‡] Simeon Bird, Marc Kamionkowski,
Julian B. Muñoz, and Alvise Raccanelli

Department of Physics and Astronomy, The Johns Hopkins University, Baltimore, Maryland 21218, USA
(Received 2 July 2016; published 6 October 2016)

It was recently suggested that the merger of $\sim 30\,M_\odot$ primordial black holes (PBHs) may provide a significant number of events in gravitational-wave observatories over the next decade, if they make up an appreciable fraction of the dark matter. Here we show that measurement of the eccentricities of the inspiralling binary black holes can be used to distinguish these binaries from those produced by more traditional astrophysical mechanisms. These PBH binaries are formed on highly eccentric orbits and can then merge on time scales that in some cases are years or less, retaining some eccentricity in the last seconds before the merger. This is to be contrasted with massive-stellar-binary, globular-cluster, or other astrophysical origins for binary black holes (BBHs) in which the orbits have very effectively circularized by the time the BBH enters the observable LIGO window. Here we discuss the features of the gravitational-wave signals that indicate this eccentricity and forecast the sensitivity of LIGO and the Einstein Telescope to such effects. We show that if PBHs make up the dark matter, then roughly one event should have a detectable eccentricity given LIGO's expected sensitivity and observing time of six years. The Einstein Telescope should see $O(10)$ such events after ten years.

I. INTRODUCTION

The LIGO collaboration recently detected gravitational waves (GWs) from the coalescence of black holes (BHs) [1,2]. Many viable models for the progenitors of coalescing binary BHs have been proposed in the literature [3–13], all consistent with the estimated rate (if all mergers involve black holes of similar masses) of Refs. [14,15]. The fact that the first detected GW signal originated from a pair of BHs with masses $\sim 30\,M_\odot$ [16] suggests that such high-mass merger events are common enough that a significant sample of them will soon be obtained.

In Ref. [3], we suggested that if $\sim 30\,M_\odot$ primordial black holes (PBH) make up the dark matter [17–19], then the rate for the merger of such events is consistent with the range inferred from the first LIGO events. PBHs in the mass range 20–100 $M_\odot$ remain viable DM candidates [20,21]—lower masses are ruled out by null microlensing searches [22–26] and pulsar-timing-array searches [27], and higher masses by the dynamics of wide stellar binaries [21,28,29]. Reference [30] inferred a strong constraint to the PBH abundance in the $\sim 30\,M_\odot$ mass range from the cosmic microwave background (CMB) spectrum and anisotropies. Reference [31] discussed an interesting constraint, from a weakly bound stellar cluster, to dark matter in this mass range. Given the caveats associated with both results, however, neither constraint is strong enough to robustly exclude the possibility of PBH dark matter. In

particular, it is conceivable, given the large number of GW events likely to be detected within the next decade, that some may be PBH binaries, even if PBHs are only a subdominant constituent of dark matter [3].

Several ideas have already been proposed to test the possibility that $\sim 30\,M_\odot$ PBHs make up all or part of the dark matter. For example, merging PBHs are likely to reside in lower-mass halos [3], so the cross-correlation of future GW event-location maps with galaxy catalogues may test the PBH-progenitor model [32,33]. The scenario may also be tested by seeking fast-radio-burst echoes induced by strong gravitational lensing by PBHs [34], or additional work along the lines of the CMB, wide-binary, or stellar-cluster probes discussed above.

In this paper we explore the possibility to distinguish directly with gravitational-wave measurements whether PBH mergers contribute some of the gravitational-wave events that will be observed. In particular, we show here that some PBH binaries through their evolution will have eccentricities that are large enough to be detectable even in the final stages of inspiral before the merger. This contrasts with the expectation for most other progenitor models, in which the orbits will have very effectively circularized by the time they reach the observable gravitational-wave window.

The velocity dispersion of dark matter PBHs in the galactic halos in which they reside depends on the size of the DM halo. For example, PBHs in Milky Way–sized halos typically have relative velocities of $O(10^2)$ km s^{-1}, while in halos as small as $10^3\,M_\odot$, those velocities are suppressed to $O(0.1)$ km s^{-1}. PBH binaries are formed

*icholis1@jhu.edu
†ekovetz1@jhu.edu
‡yacine@jhu.edu

when two PBHs pass so close that they emit enough energy to GW radiation to form a bound pair. Higher relative velocities result in tighter binaries with highly eccentric (nearly parabolic) orbits. As the PBHs coalesce, the orbit will gradually circularize. The characteristic merger time, though, can vary significantly, leading to a wide range of residual orbital eccentricities, as different merger events enter the frequency band of a GW detector. The signature of higher eccentricities is the observation of the higher harmonics they produce in the gravitational-wave signal. Here we focus, in particular, on the possibility of observing these higher harmonics with advanced LIGO [35] and the planned Einstein Telescope (ET) [36]. We find that the former is likely to see $O(1)$ and the latter $O(10)$ such eccentric mergers of $\sim 30\ M_\odot$ BHs over the span of ten years, providing an important test of the PBH scenario.

Before proceeding, we note that Refs. [37,38] have argued for mechanisms by which PBHs would form binaries in the early Universe. Reference [38] concluded that PBHs would be compatible with the observed LIGO GW150914 event-type rate while making up only a fraction of the dark matter. The mergers of such primordial PBH binaries would occur only after the primordial binaries have had considerable opportunity to circularize. The large-eccentricity signature of PBHs that we discuss here thus applies only to the scenario envisaged in Ref. [3], in which PBH binaries form late in the Universe via GW radiation.

This paper is organized as follows. In Sec. II we review the two-body GW mechanism for binary capture, as well as the equations for the evolution of the orbital properties during the subsequent merger. In Sec. III we analyze the case of PBH binaries and calculate their initial orbital properties and their evolution, including the time from formation until merger and their final eccentricities. We discuss also the effects that a third body may have on the existing PBH binaries. In Sec. IV we address the detectability of the high-eccentricity PBH-merger events by current and future GW observatories. We first estimate the expected event rate for eccentric events and compare it to other progenitor models for the formation of BBHs that, in particular, occur at globular clusters (GCs) or in environments near supermassive BHs. Furthermore we consider the resulting gravitational-wave modes and their observational consequences. We conclude in Sec. V.

II. PRELIMINARIES

In this section we provide the formulas that are used to derive our results in Sec. III. Unless explicitly specified we use geometric units with $G = c = 1$.

A. Two-body binary capture

We consider the formation of a binary from two BHs with masses m_1 and m_2 and a mass ratio defined as

$$\eta(m_1, m_2) = \frac{m_1 m_2}{(m_1 + m_2)^2} \equiv \frac{m_1 m_2}{m_{\text{tot}}^2}. \tag{1}$$

As the two BHs approach each other with a relative velocity w, they emit gravitational waves whose power peaks at r_p, the distance of closest approach, which is related to the impact parameter b by [39]

$$b = \frac{\sqrt{2 m_{\text{tot}} r_p}}{w} \left(1 + \frac{r_p w^2}{2 m_{\text{tot}}} \right)^{1/2} \text{ or to first order in } w/c,$$

$$r_p(m_1, m_2, w, b) \simeq \frac{b^2 w^2}{2 m_{\text{tot}}} \left(1 - \frac{b^2 w^4}{4 m_{\text{tot}}^2} \right). \tag{2}$$

In order for the two BHs to create a binary after the close encounter, enough energy has to be radiated via GWs. For such systems, the *final* energy right after formation is given by [40,41]

$$E_f(m_1, m_2, w, b) = \frac{m_{\text{tot}} \eta w^2}{2} - \frac{85\pi}{12\sqrt{2}} \frac{\eta^2 m_{\text{tot}}^{9/2}}{r_p^{7/2}}, \tag{3}$$

where the second term is the energy released in GWs, and the maximum impact parameter to form a bound binary is [39]

$$b_{\text{max}}(m_1, m_2, w) = \left(\frac{340\pi}{3} \right)^{1/7} \frac{m_{\text{tot}} \eta^{1/7}}{w^{9/7}}. \tag{4}$$

Once formed, the binary's initial semimajor axis is

$$a_0(m_1, m_2, w, b) = -\frac{m_{\text{tot}}^2 \eta}{2 E_f}, \tag{5}$$

while its initial eccentricity is

$$e_0(m_1, m_2, w, b) = \sqrt{1 + 2 \frac{E_f b^2 w^2}{m_{\text{tot}}^3 \eta}}, \tag{6}$$

and the initial Keplerian-orbit pericenter distance is given by $r_{p_0} = a_0(1 - e_0)$, or in its dimensionless parametrization, $\rho_{p_0} = r_{p_0}/m_{\text{tot}}$.

It is useful in what follows to rewrite these expressions as a function of $b/b_{\text{max}}(w)$,

$$E_f = -\frac{1}{2} m_{\text{tot}} \eta w^2 \left[\left(\frac{b_{\text{max}}}{b} \right)^7 - 1 \right], \tag{7}$$

$$a_0 = m_{\text{tot}} w^{-2} \left[\left(\frac{b_{\text{max}}}{b} \right)^7 - 1 \right]^{-1}, \tag{8}$$

$$1 - e_0^2 = \left(\frac{340\pi\eta}{3} \right)^{2/7} w^{10/7} \left(\frac{b}{b_{\text{max}}} \right)^2 \left[\left(\frac{b_{\text{max}}}{b} \right)^7 - 1 \right]. \tag{9}$$

B. Merger time scale and orbital evolution

For a binary with initial eccentricity $e_0 \simeq 1$ and semimajor axis a_0, the time it takes it to merge is given by [42]

$$\tau_m(m_1, m_2, e_0, a_0) = \frac{15}{19} \left(\frac{304}{425}\right)^{\frac{3480}{2299}} \frac{m_{\text{tot}} \rho_{p_0}^4}{4\eta}$$
$$\times \int_{e_{\text{LSO}}}^{e_0} de\, e^{29/19} \frac{(1 + \frac{121}{304} e^3)^{\frac{1181}{2299}}}{(1 - e^2)^{3/2}}. \quad (10)$$

Given that e_0 and a_0 can be traced back to the initial relative velocity and impact parameter of the BHs, Eq. (10) can be recast as

$$\tau_m(m_1, m_2, w, b) = \frac{3}{85} \frac{a_0^4}{m_{\text{tot}}^3 \eta} (1 - e_0^2)^{7/2}. \quad (11)$$

Thus in our analysis of PBH binaries, we simply need to simulate the distributions of w and b for a given choice of m_1 and m_2. This is done in the next section.

In order to track the evolution of the orbital eccentricity, we evolve the BH binaries until their final eccentricity e, given an initial value e_0, some initial pericenter distance r_{p_0} and a final pericenter distance r_{p_f}. The semimajor axis and eccentricity decrease due to angular momentum and energy loss through gravitational-wave radiation. The resulting coupled ordinary differential equations can be rewritten as

$$r_p \frac{de}{dr_p} = e(1 + e) \frac{304 + 121e^2}{192 - 112e + 168e^2 + 47e^3}. \quad (12)$$

This equation can be integrated analytically and the solution takes the form of an algebraic equation [42]

$$\frac{r_p}{r_{p_0}} = \left(\frac{e}{e_0}\right)^{12/19} \frac{\mathcal{F}(e)}{\mathcal{F}(e_0)}, \quad (13)$$

with

$$\mathcal{F}(e) \equiv (1 + e)^{-1} \left(1 + \frac{121}{304} e^2\right)^{\frac{870}{2299}}. \quad (14)$$

We wish to find the eccentricity e_f when the pericenter reaches some final value r_{p_f}. Equation (13) is implicit in e_f,

$$e_f = e_0 \left(\frac{r_{p_f}}{r_{p_0}} \frac{\mathcal{F}(e_f)}{\mathcal{F}(e_0)}\right)^{19/12}. \quad (15)$$

However, it can be solved very efficiently through the following iterative method: we set $e_f^{(0)} \equiv 0$ and

$$e_f^{(i+1)} \equiv e_0 \left(\frac{r_{p_f}}{r_{p_0}} \frac{\mathcal{F}(e_f^{(i)})}{\mathcal{F}(e_0)}\right)^{19/12}. \quad (16)$$

We iterate until reaching a 1% convergence. We have checked that the solution obtained this way matches that obtained from explicitly solving Eq. (12).

III. THE CASE OF DM PBH BINARIES

A. Assumed distributions of PBHs in DM halos

In deriving the distribution functions for PBHs in DM halos, we have to make some assumptions regarding the velocity distribution of the PBHs. Following [3], we take a Maxwell-Boltzmann distribution,

$$P_{v_{\text{PBH}}}(v) = F_0^{-1} v^2 (e^{-v^2/v_{\text{DM}}^2} - e^{-v_{\text{vir}}^2/v_{\text{DM}}^2}), \quad (17)$$

with $F_0 = 4\pi \int_0^{v_{\text{vir}}} v^2 (e^{-v^2/v_{\text{DM}}^2} - e^{-v_{\text{vir}}^2/v_{\text{DM}}^2})$ and where the velocity dispersion v_{DM} and the virial velocity v_{vir} depend on the DM halo mass. For a $10^{12}\, M_\odot/h$ object for instance, we have $v_{\text{DM}} = 166$ and $v_{\text{vir}} = 200$ km s^{-1}. The typical relative velocity of PBHs in a $10^6 (10^9, 10^{12})\, M_\odot/h$ DM halo is $w = \sqrt{2}v = 2(\times 10^1, \times 10^2)$ km s^{-1}, and for $m_1 = m_2 = 30\, M_\odot$, we get $b_{\text{max}} = 5.1\ (0.26, 1.3 \times 10^{-2})$ au.

As for the impact parameter, we assume that b^2 is uniformly distributed between 0 and $b_{\text{max}}^2 (30\, M_\odot, 30\, M_\odot, w)$.

Using these distributions, we simulate the formation of 10^6 binary PBHs of $30\, M_\odot$. Their rate of formation in a DM halo of a given mass is described in Eqs. (8) and (9) of Ref. [3], where it was shown that the total rate of merging PBH binaries overlaps with the range of 2–53 per Gpc^3 per yr quoted by LIGO [15]. Recently, the rate of $\sim 30\, M_\odot$ merging black holes was reevaluated to be between 0.5 and 11.5 mergers per Gpc^3 per yr [14]. In the remainder of the paper we normalize the rate of PBH to this updated observed LIGO rate.

B. Initial inspiral properties

The probability distribution functions (PDFs) for the eccentricity at binary formation are shown in Fig. 1, where we present our results for binaries residing in three different sizes of DM halos, i.e. virial masses of 10^6, 10^9 and 10^{12} $M_\odot/h$. We find that in all cases the eccentricity of the BHs is close to unity at formation regardless of the mass of the host halo. In fact, a heuristic argument can be made for where the peak of the PDF of the eccentricity distribution, $(1 - e_0)^{\text{peak}}$, should be. The $(1 - e_0)^{\text{peak}} = r_{p_0}/a_0$ which from Eqs. (2) (at zeroth order) and (5) is $-b^2 w^2 E_f/(m_{\text{tot}}^3 \eta)$. Approximating b with b_{max} [given by Eq. (4)], we get $(1 - e_0)^{\text{peak}} \simeq -(340\pi/3)^{2/7}\, w^{-4/7} \eta^{-5/7} E_f/m_{\text{tot}}$. Since the initial energy of the system is $E_i = \eta m_{\text{tot}} w^2/2$, and defining $\xi = |E_f|/E_i$, this gives $(1 - e_0)^{\text{peak}} \simeq 2.6 \xi \eta^{2/7} (w/c)^{10/7}$. Matching to the peaks in the simulations, shown in Fig. 1, they fall at $\xi \simeq 1$ for $w = 2(\times 10^1, \times 10^2)$ km s^{-1}. As we discuss below, binary BHs created dynamically in globular clusters have flatter eccentricity distributions at formation.
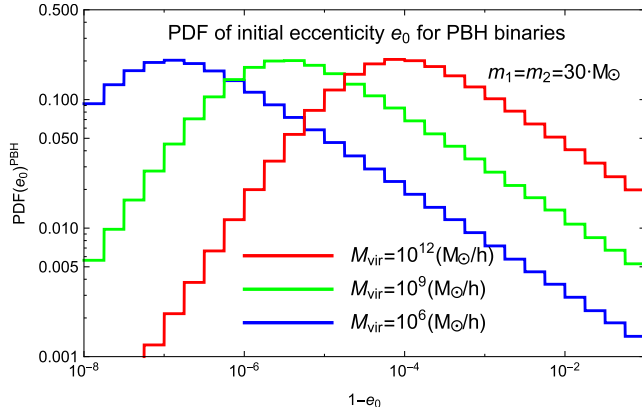
FIG. 1. The distribution PDF(e_0) of eccentricities at formation, for PBH binaries residing in DM halos of three different sizes, based on 10^6 simulations. In *all cases* the PBH binaries have highly eccentric orbits, with their respective distributions peaking as expected (see the text for details).

The PDFs for the semimajor axis, the initial pericenter distance and the time τ_m from formation until merger are shown in Figs. 2–4, respectively. Here again, we can derive simple scalings analytically. From Eqs. (8) and (11) we get, for $m_{tot} = 60\ M_\odot$,

$$a_0 \sim m_{tot} v_{DM}^{-2} \sim 100\ \text{au}\ (v_{DM}/20\ \text{km s}^{-1})^{-2}, \quad (18)$$

$$r_{p_0} = a_0(1 - e_0) \sim 2 \times 10^4\ \text{km}\ (v_{DM}/20\ \text{km s}^{-1})^{-4/7}, \quad (19)$$

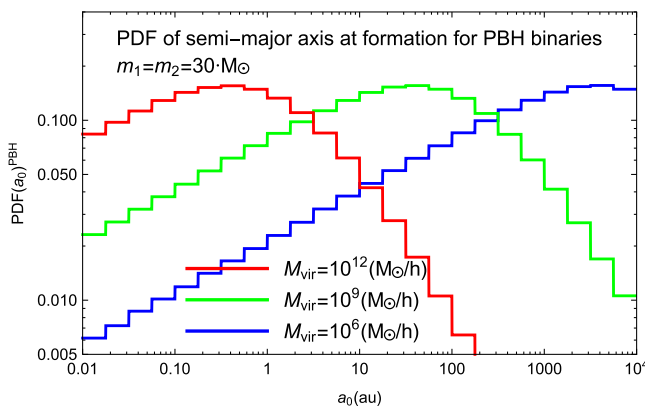$$\tau_m \sim 10^9\ \text{s}\ (v_{DM}/20\ \text{km s}^{-1})^{-3}. \quad (20)$$

FIG. 2. The distribution PDF(a_0) of the semimajor axis a_0 at formation. We consider PBH binaries residing in DM halos of three different sizes. The formed binaries in larger halos have smaller distance separation. Even for PBH binaries in $10^6\ M_\odot$ halos, a_0 only goes up to $O(10^4)$ au. In all cases we used 10^6 simulated BH binaries.
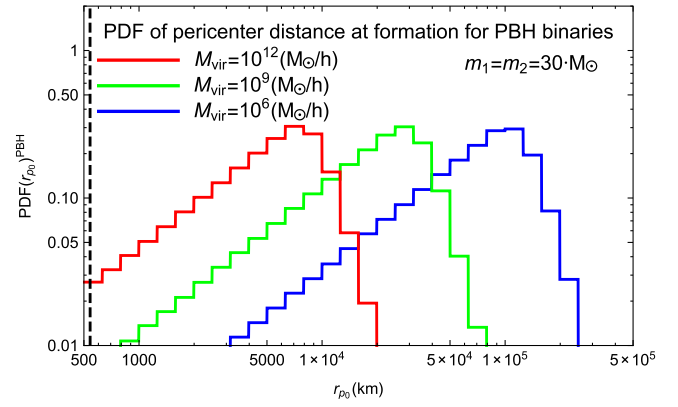

FIG. 3. The distribution of the pericenter distance r_{p_0} at binary formation PDF(r_{p_0}). As in Figs. 1 and 2, we show binary PBHs residing at three different DM halo sizes. Some of the formed PBH binaries at Milky Way–sized and dwarf galaxy sized halos have pericenter distances at formation very close to (and even in some cases less than) the last stable orbit distance of 6 R_{Sch} (black dashed line), suggesting direct plunges. In all cases we used 10^6 simulated BH binaries.

These quantities depend strongly on the DM halo the binaries form in. Due to the difference in velocity dispersions between halos of different masses, the characteristic time it takes a BH binary to merge can range from minutes to hours for $M_{vir} \simeq 10^{12} M_\odot/h$ up to 100 kyrs for $M_{vir} \simeq 10^6 M_\odot/h$. In environments with high relative velocities the capture rate is much smaller, as was shown in Ref. [3], but when such captures occur they result in tight binaries that merge much faster. For any choice of parameters, the merger time scales for PBH binaries are always small enough that the evolution of the DM halo during the coalescence can be neglected. Therefore, the
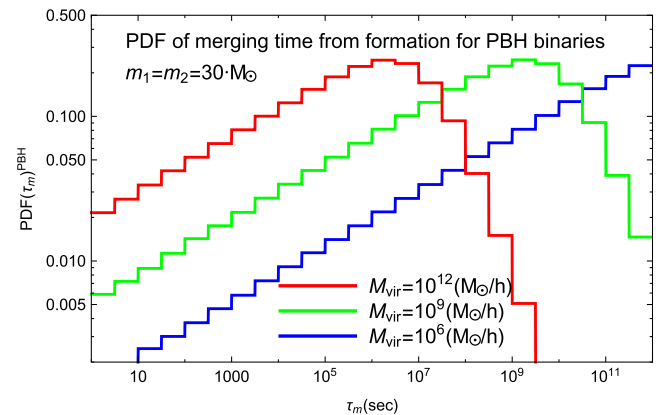

FIG. 4. The distribution PDF(τ_m) of time between binary formation and merger, considering host DM halos of three different sizes. Binaries of PBHs in Milky Way–like halos tend to merge within months ($\lesssim 10^7$ s) of their formation, with a significant portion merging within hours ($\lesssim 10^4$ s). Even for PBH binaries in $10^6\ M_\odot$ halos, there is a few percent chance that they merge within hours of their formation.

merger rate can be taken to equal the rate of PBH binary formation. This is generally not the case for binaries formed in other astrophysical environments where the initial separations are typically larger and the merger time scales can be as large as Gyrs [8,43–51]. This difference in merger time scales is an essential characteristic in discriminating between the PBH and other progenitors.

If the impact parameter is small enough, the pericenter at first passage can be less than $6R_{\text{Sch}}$, the radius of the innermost stable orbit (R_{Sch} is the Schwarzschild radius of the 30 $M_\odot$ PBHs). In this case the BHs practically collide (plunge) at first encounter. Such events would also produce strong GW signals. However, these would not follow the same waveform evolution as typical coalescence events currently searched for by LIGO. Based on Eq. (2) to lowest order in w, we see that this corresponds to a minimum impact parameter,

$$b_{\text{min}}(w) = \sqrt{12}\, m_{\text{tot}} w^{-1} = \sqrt{12}\left(\frac{3}{340\pi\eta}\right)^{1/7} w^{2/7} b_{\text{max}}(w). \tag{21}$$

The fraction of binary formation events that are direct plunges is therefore of order

$$(b_{\text{min}}/b_{\text{max}})^2 \sim 12\left(\frac{3}{340\pi\eta}\right)^{1/7} v_{\text{DM}}^{4/7}$$
$$\sim 1\%(v_{\text{DM}}/20\ \text{km s}^{-1})^{4/7}. \tag{22}$$

Numerically, we find that for PBHs of 30 $M_\odot$ residing in 10^6 (10^9, 10^{12}) $M_\odot/h$ 0.3% (1.3%, 4%) of the interactions for which $E_f < 0$ fall in that category.

Figures 1–4 do include those plunges. To search for such events, a better understanding of the expected signals is needed, most likely through numerical-relativity simulations. In the remainder of the paper we exclude such plunge events when referring to BH binary mergers.

C. Final eccentricities

Following the binary evolution until the last stable orbit of $6R_{\text{Sch}}$, we derive their final eccentricity distribution in Fig. 5. We show the distributions of eccentricities for three different pericenter distances. These are at 22, 14 and 6 R_{Sch}. We choose 22 R_{Sch} as this is the distance at which we estimate the binary to enter the LIGO band of observations: a pair of 30 $M_\odot$ BHs will merge at an orbital frequency of $\simeq 35$ Hz ($\simeq 70$ Hz for the quadrupole mode). LIGO at final design will be able to detect down to orbital frequencies of 5 Hz (or quadrupole frequencies of 10 Hz). Thus LIGO with enough sensitivity can observe such a system's orbital period evolution out to a factor of 7. Using Kepler's third law of motion, this results in a semimajor axis evolution by a factor of $7^{2/3} = 3.7$. For fixed eccentricity, the pericenter distance will evolve by the
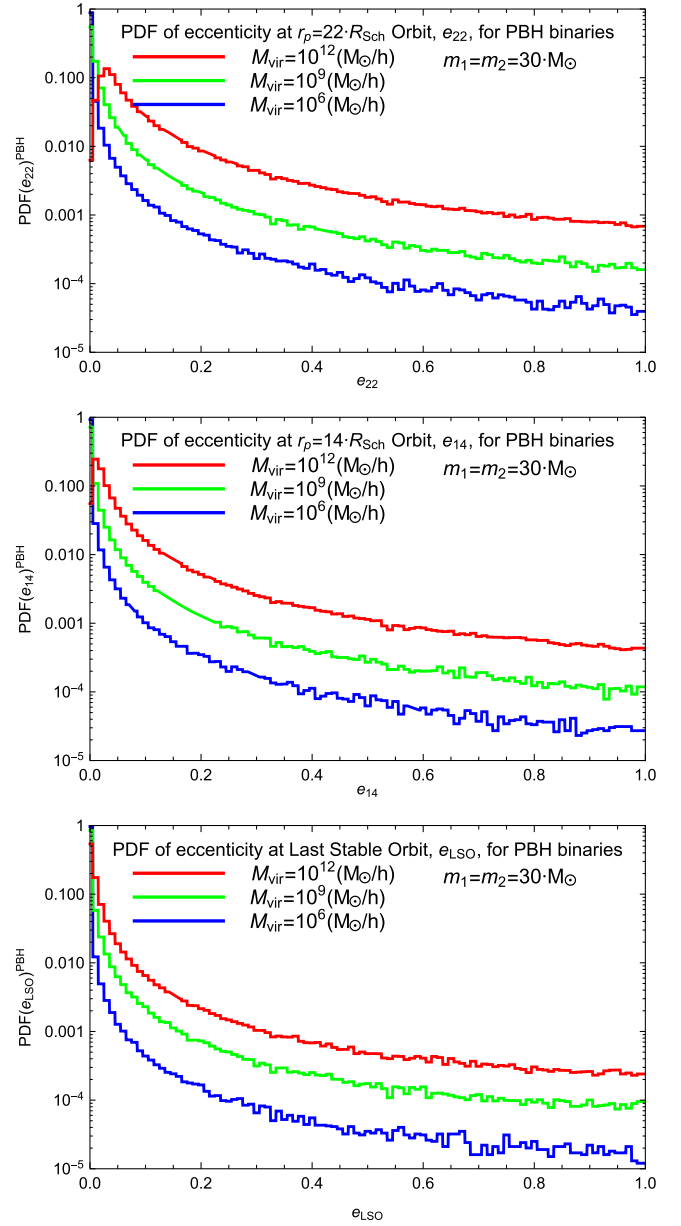

FIG. 5. The distribution of eccentricities at three different pericenter distances for PBHs. The eccentricities e_{22}, e_{14} and e_{LSO} refer to the orbital eccentricity when the pericenter distance r_p is 22, 14 and 6 R_{Sch}, respectively, near enough to enter the LIGO and ET observed frequency bands. As before, we show results for three different host-halo masses. PBH binaries in Milky Way–sized halos, although they have a much lower formation rate, retain higher eccentricities up to the latest stages (due to the smaller impact parameter required for their formation). PBH binaries residing at 10^6 $M_\odot/h$ have a ~0.1% chance to remain in an eccentric orbit up to the late stages.

same factor, i.e. from $3.7 \times 6 = 22$ R_{Sch} to 6 R_{Sch}. Realistically, since the eccentricity will also be reduced, the evolution in the pericenter distance is smaller. The value of 14 R_{Sch} is thus also presented as an intermediate case.

Figure 5 in combination with Fig. 4 suggests that binaries in heavier DM halos retain their high values of eccentricities due to their quick merger time τ_m. The connection between τ_m and final eccentricity e_{LSO} (e_{14}, e_{22}) can be seen even more clearly in Fig. 6, where we plot contours with the recurrence of these PBH binary properties. We use 30 $M_\odot$ residing in 10^{12} $M_\odot/h$ DM halos. We have checked that allowing the PBH mass to vary anywhere in the range 20–40 $M_\odot$ does not affect either the time scale or the eccentricity results beyond the 10% level. Observationally, LIGO and future detectors will probe a combination of all the narrow bands of Fig. 6, since it will be difficult to define an eccentricity at a specific pericenter distance, given the fast evolution of the binary's orbital properties at the late inspiral stages.

Finally, we comment on the impact of a third PBH on the existing binaries and their properties. A third BH traveling with a relative velocity w' will affect significantly the binary if it comes within a distance similar to its semimajor axis $a \leq a_0$. The time scale for that is $\tau_{3rd} \sim (\pi a_0^2 w' n_{BH})^{-1}$, with n_{BH} being their local halo density. We compare that time scale to the binary merger time scale τ_m. The ratio of $\tau_m/\tau_{3rd} \sim \pi a_0^2 w' n_{BH} \tau_m$. Using Eq. (11) and the results in Sec. III B, we get $\tau_m/\tau_{3rd} \sim m_{BH}^3 w'^{-6} n_{BH}$. Since $w' \sim (M_{halo}/R_{halo})^{1/2}$ and $n_{BH} \sim M_{halo}/V_{halo}$ (M_{halo}, R_{halo} and

V_{halo} are the mass, scale radius and volume of the DM halo), we get that $\tau_m/\tau_{3rd} \sim N^{-2}$ where N is the number of PBHs in the DM halo. We assume that even for the smallest halos $N \geq 13$. Thus third-body interactions are negligible. Another possible effect includes the likely rare occasion at which a third BH of mass m_3 orbits the tight binary, causing eccentricity oscillations with a time scale τ_{osc} of [52,53]

$$\tau_{osc} = P \frac{m_1 + m_2}{m_3} \left(\frac{a_2}{a_1}\right)^3 (1 - e_2^2)^{3/2}. \qquad (23)$$

P is the orbital period of the tighter binary, a_1 the semimajor axis of the tight binary and a_2 and e_2 the equivalent orbital quantities for the binary-third BH system. Here $m_1 = m_2 = m_3$. Considering first $10^6(10^3)$ $M_\odot/h$ DM halos, we take for a_1 the characteristic initial values a_0 of $3 \times 10^3 (\times 10^5)$ au, since the slowest evolution of any binary's orbital properties occurs at the beginning of its existence. For a_2 we take the equivalent typical separation distance between BHs in the halos of $2(0.5) \times 10^6$ au. Assuming also that $e_2 \ll 1$, we get based on Eq. (23) that $\tau_{osc}/P = 1.5 \times 10^8(70)$ for binaries in 10^6 (10^3) $M_\odot/h$ DM halos. These numbers refer to the τ_{osc}/P ratio at the beginning of the tight binary's existence. As the binary evolves its semimajor axis a_1 get reduced, while the typical separation distance between BHs remains the same; thus the impact of the eccentricity oscillations becomes less relevant during the evolution of the binary. In more massive halos the τ_{osc}/P ratios are even larger. Furthermore, for the events that give high remaining eccentricities, the τ_{osc}/P ratios are even higher than the typical values calculated above, since the relevant a_1 values are smaller in those binaries. Thus we conclude that even if a significant fraction of binaries had a third BH orbiting around, eccentricity oscillations can be ignored in this work as well.
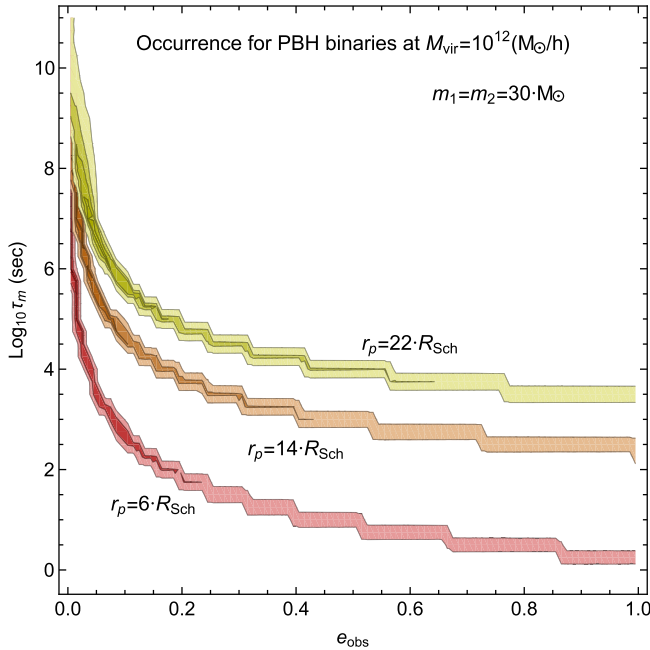
IV. DETECTABILITY

The detectability of an eccentric PBH-binary inspiral will depend on the exact level of the eccentricity before the last stable orbit (for a given noise level), as well as its distance from Earth. High values of eccentricities can be probed with current as well as future detectors, as we discuss next. We begin with an estimation of the event rate for elliptical orbits and then discuss the expected gravitational waves from these mergers.

A. Eccentric event rates

In Table I, we present the calculated fraction of 30 $M_\odot$ PBHs with eccentricities e_{22}, e_{14} and e_{LSO} of at least 0.1, 0.2, 0.3 or 0.5, respectively. We find that for PBHs in dark matter halos of virial mass larger than 10^6 $M_\odot$, those fractions are more than $O(0.01)$. Even for PBH binaries in less massive halos the fraction is always more than 2×10^{-3}.

FIG. 6. The distribution of time τ_m between binary formation and merger versus the e_{22}, e_{14} and e_{LSO} eccentricities, for binaries of PBHs residing in 10^{12} $M_\odot/h$. Color brightness indicates the occurrence of binaries. We show regions including 33%, 68%, 95% and 99.5% of the 10^6 simulated BH binaries. Binaries with merging times of more than 10 yrs do not retain eccentricities larger than 0.05 by the time they enter the LIGO band.

TABLE I. The typical values for the fractions of eccentric orbits at the late stages of inspirals, assuming 30 $M_\odot$ PBH binaries. For each case we provide three numbers, referring to the eccentricities at pericenter distances $r_p = 6$, 14 and $22R_{Sch}$, respectively. In the last column, we show the fraction of events for which the initial pericenter distance r_{p_0} is smaller than the r_p threshold.

Environment M_{vir} ($M_\odot/h$)	% fraction with $e_{obs} > 0.1$	% fraction with $e_{obs} > 0.2$	% fraction with $e_{obs} > 0.3$	% fraction with $e_{obs} > 0.5$	% fraction with $r_{p_0} < r_p$
PBHs in 10^3	0.2, 0.4, 0.6	0.1, 0.2, 0.3	0.06, 0.12, 0.19	0.03, 0.06, 0.10	0.05, 0.15, 0.23
PBHs in 10^6	0.6, 1.3, 2.0	0.3, 0.7, 1.1	0.2, 0.4, 0.7	0.1, 0.2, 0.3	0.3, 0.5, 1.0
PBHs in 10^9	2.6, 5, 8	1.5, 2.5, 4	1.0, 1.6, 2.5	0.5, 0.8, 1.2	1.3, 2.2, 4
PBHs in 10^{12}	8, 18, 29	5, 10, 15	3, 6, 10	1.5, 3, 5	4, 9, 15

For LIGO we assume that eccentric events with $e_{14} > 0.3$ would be observable up to a redshift of 0.75 at final design sensitivity. The expected number of observed events with e_{obs} up to a redshift z_{max} is given by

$$N^{e_{obs}} = T_{obs} \int_0^{z_{max}} dz \frac{R_m^{e_{obs}}(z) 4\pi\chi^2(z)}{(1+z)H(z)}, \qquad (24)$$

where $R_m^{e_{obs}}(z)$ is the comoving merger rate of eccentric events with e_{obs} at the source redshift, $\chi(z)$ is the comoving distance and T_{obs} is the observing time. Our results are shown in Table II for $e_{obs} = e_{14}$. After 6 years of LIGO final-design observations, we expect a total of $O(1)$ events with $e_{14} > 0.2$, none of which would originate in dark matter halos more massive than $10^6 M_\odot$. We also show forecasts for the ET, for which the exact design sensitivity has yet to be determined. Thus, we project for two alternative values, $z = 3$ and 10 ("optimistic"), of the maximum redshift to detect eccentric events with $e_{14} > 0.1$. ET may observe up to a few events originating in $10^6 M_\odot$ halos, and once integrating over the entire halo mass range considered, that number increases to $O(10)$.

The GW event contribution from the least massive halos has significant uncertainties. These originate from our assumptions about the DM profile (at the level of a factor of 2), the concentration-mass relation (by another factor of 2), and also from discreteness effects of PBH DM. For further details on the PBH event rates, we refer the reader to

the discussion in [3]. These uncertainties result in a wide range of predictions for the rate of PBH mergers, compatible with the updated LIGO rate of 0.5–11.5 Gpc^{-3} yr^{-1}, mentioned in Sec. III A. In Table II we used the updated LIGO range for the total rate of PBHs. For redshifts $z > 6$, relevant for the optimistic ET projections, the mass-concentration relations [54,55] are not properly calibrated. Thus, extending them to predict rates at high redshifts may result in additional uncertainties. We note that if instead of the fixed value 30 $M_\odot$ for the PBHs, their mass is allowed to be in the wider range of 20–40 $M_\odot$, the number of eccentric coalescence events presented in Table II changes by only $\simeq 10\%$, increasing with decreasing BH mass.

B. Alternative models to PBHs

As mentioned in the introduction, there are a number of alternative models for the progenitors of BH binaries whose mergers may be seen in gravitational-wave observatories. For example, GCs may provide fertile breeding grounds for binary black holes. Most binaries in GCs are formed by three-body interactions, where the BHs form a binary that becomes tighter after multiple interactions with nearby BHs over a time span of Gyrs. Moreover, through those same interactions the binaries receive random kicks, and eventually get ejected from their host GC [8,56], after which they evolve as isolated systems. As a consequence, these systems are typically highly circularized well before their

TABLE II. The typical numbers of eccentric orbits at the late stages of inspiral for alternative conditions on the host halo of 30 $M_\odot$ PBHs. The rate quoted is the comoving merger rate. In the last three columns we present the number of events we expect LIGO (final design) or ET would observe in a 6 or 10 year interval, respectively. The values in the last column account for optimistic alternative assumptions regarding the ET sensitivity (see the text for details). For the case where we include all PBHs in halos of $10^{2.5} M_\odot/h$ or heavier (fourth row), we give a range in accordance to the LIGO quoted rate. The relative contribution from different DM halos is based on the results of [3]. In the bottom row we show the expected contribution from two-body encounters of BHs in the cores of globular clusters, with uncertainty ranges reflecting the major astrophysical uncertainties (see the text for details).

Environment M_{vir} ($M_\odot/h$)	$R_m(0)^{e_{14}>0.2}$ (Gpc^3 yr^{-1})	$N^{e_{14}>0.2}$ LIGO 6 yr	$N^{e_{14}>0.1}$ ET 10 yr	$N^{e_{14}>0.1}$ ET 10 yr (optimistic)
PBHs in 10^6	$(0.2\text{–}4) \times 10^{-4}$	$(0.05\text{–}1) \times 10^{-1}$	0.04–1	0.08–2
PBHs in 10^9	$(0.1\text{–}2.5) \times 10^{-5}$	$(0.2\text{–}5) \times 10^{-3}$	$(0.2\text{–}4) \times 10^{-2}$	$(0.5\text{–}10) \times 10^{-2}$
PBHs in 10^{12}	$(0.7\text{–}20) \times 10^{-7}$	$(0.15\text{–}3) \times 10^{-5}$	$(0.25\text{–}5) \times 10^{-3}$	$(0.04\text{–}0.8) \times 10^{-2}$
PBHs in $> 10^{2.5}$	$(1\text{–}20) \times 10^{-3}$	0.3–5	1.5–30	3–60
BHs in GC^{2body}	$(0.2\text{–}2) \times 10^{-5}$	$(1\text{–}10) \times 10^{-3}$	0.1–1	0.3–5

GW emission enters the LIGO sensitivity band [5,57] (see though [53,58] for three-body systems where the tighter BH-BH binary may go through eccentricity oscillations). However, there is a small fraction of BH binaries formed through two-body interactions at the cores of GCs, which may retain their eccentricities up to the last stages of the inspiral. We study these binaries, and refer to them as BHs in GC^{2body} (fifth row in Table II).

A representative distribution of the structural parameters of GCs can be found on the Harris catalog [59]. We focus on the objects of this catalog with a measurement of their core velocity dispersion. For these GCs we can also retrieve their core radii, distributed log normally around 1 pc, and their core luminosities. We calculate the GC core mass from its luminosity, assuming a light-to-mass ratio of 1 $L_\odot/M_\odot$. Given these three parameters, we can calculate the number of two-body captures that would occur in a GC core [39], assuming that BHs make up all its mass. We find this binary formation rate to be between $\sim 10^{-10}$ and 10^{-11} yr^{-1} per GC, for GCs with core radii in the range from 0.1 to 1 pc. Smaller cores would not have enough BHs to have any meaningful interactions, and bigger cores would be too diffuse.

However, not all of the core mass will be in the form of BHs. With the Kroupa initial mass function [5,60], only 1% of the mass of the entire GC is in objects heavier than 30 $M_\odot$. The core mass is around one tenth of the total GC mass, thus yielding an upper estimate of $f_{BH} \simeq 0.1$ to the fraction of the core mass in 30 $M_\odot$ BHs (that is if all the 30 $M_\odot$ BHs of a GC are concentrated in its core). Knowing f_{BH}, and since there are roughly 0.7 GCs per Mpc^3 [61], we obtain a local merger rate of $R_m(z=0) = 7 \times 10^{-2} - 7 \times 10^{-3} \times f_{BH}^2$ Gpc^{-3} yr^{-1}. We note that this rate is a realistic upper bound. Many effects can change it. Many BHs from stars more massive than 30 $M_\odot$ end up becoming lighter BHs, which should not be confused with the PBHs that we are after. Moreover, it has been suggested that heavy BHs are expelled from GCs early on [5]. Alternatively, dynamical friction can bring the velocity dispersion of the BHs below that of the stars in the GC core, decreasing their virial radius and making them more concentrated, hence producing more events.

Of course, not all the BH mergers due to two-body interactions in the cores of GCs will be highly eccentric. To find the number of these events we have assumed that the BHs follow a Maxwell-Boltzmann relative velocity distribution with $v_{DM} = 12$ km s^{-1} [59]. Thus, while GCs can in fact be the major source of GW detections, coming from circular BH binaries, we do not expect LIGO to observe any heavy binary mergers with high eccentricities [we estimate less than $O(10^{-2})$ events]. With ET, and after 10 yrs of observations, there is an optimistic estimate of $O(1)$ eccentric events from GCs, to be compared to the conservative $O(10)$ events from PBHs. We think that these two alternatives remain distinguishable.

The authors of Ref. [39] have suggested another scenario for binary BHs with eccentric inspirals in the LIGO frequency range. These binaries reside in the inner sub-pc of galactic nuclei and are formed by two-body interactions of BHs in a gravitational potential dominated by the central supermassive BH. Such black hole binaries, with relative velocities of $\simeq 30$–80 km s^{-1}, would also be formed with high initial eccentricities and relatively small merger time scales. We get that $\simeq 10\%$ of such binaries would retain a high eccentricity. However, the model of Ref. [39] relies on densities of BHs that are extremely uncertain in the inner sub-pc of the galactic nuclei, with those densities varying by typically ~ 10 orders of magnitude (20 orders of magnitude for the rate profile) from 10^{-4} to 1 pc. In particular, using the models "B" and "E-2" of [39] for which a density profile is given, we find that $\simeq 60\%(\simeq 95\%)$ of the total merger rates are due to $O(10)$ [$O(10^2)$] BHs in the inner $10^{-3}(10^{-2})$ pc.

In our opinion, all these uncertainties are simply too large to allow a fair comparison to the PBHs case. Yet, we note that if one takes their assumptions at face value, then LIGO should be able to detect anywhere between a few to several hundreds of eccentric events during its expected observation period, with a factor of 10 more total (nearly circularized) events. Yet, all those events should still follow a mass function, originating from the initial stellar mass function, with the majority of those events being 5–10 $M_\odot$ merging BHs. That is in stark contrast to the narrower and higher mass range of the PBHs considered here.

C. Waves from eccentric inspirals

In the previous section we discussed the properties of PBH binaries and the rate of occurrence of gravitational-wave inspirals with high eccentricities, showing that with fiducial assumptions we could perhaps observe such events with LIGO. In this section, we discuss some observational aspects of these high-eccentricity events.

Every coalescence event has an inspiral phase lasting τ_m, a merger phase, and a ringdown phase. Each observatory can, through the portion of the inspiral phase that is within its frequency range, measure the redshifted chirp mass, which at the position of the source is

$$M_c = \frac{(m_1 \cdot m_2)^{3/5}}{m_{tot}^{1/5}}. \tag{25}$$

Following Ref. [62], the spectral energy density at the source of the emitted GWs during the inspiral of a circularized orbit is

$$\frac{dE}{df_s}\bigg|_{inspiral} = \frac{1}{3}\left(\frac{\pi^2}{f_s}\right)^{1/3}\frac{m_2 \cdot m_2}{m_{tot}^{1/3}}, \tag{26}$$

where f_s is the GW frequency at the source ($f_{obs} = f_s/(1+z)$). The frequency at the end of the inspiral and the beginning of the merger phase is (at the source)

$$f_{\text{merger}}(m_1, m_2) = 0.02/m_{\text{tot}}. \qquad (27)$$

Between the redshifted f_{merger} and the frequency of quasinormal ringdown (at the position of the binary),

$$f_{\text{ringdown}}(m_1, m_2) = \frac{(1 - 0.63(1 - \alpha)^{3/10})}{2\pi m_{\text{tot}}}, \qquad (28)$$

the merger phase of the coalescence events is observed. The dimensionless spin α of the final BH is simply $\alpha = \frac{cS}{Gm_f^2}$, assuming $m_f \simeq m_{\text{tot}}$. The merger phase is taken to last

$$\tau_{\text{merger}}(m_1, m_2) = 14.7 \frac{m_{\text{tot}}}{10^5 \, M_\odot} \, \text{s}. \qquad (29)$$

During the merger phase, the spectral energy density is given by

$$\frac{dE}{df_{s\,\text{merger}}} = \frac{16\mu^2 \epsilon}{m_{\text{tot}}(f_{\text{ringdown}} - f_{\text{merger}})}, \qquad (30)$$

where μ is the reduced mass and ϵ is the fraction of the energy in the initial BH binary that is emitted in GWs during the merger phase. We take $\epsilon = 0.04$, in agreement with the uncertainties of the GW150914 event [16]. Alternative values for ϵ and α only affect the merger and ringdown phases, which are of no direct importance for the eccentricity discussion here.

The observed strain amplitude is

$$h_c(f_{\text{obs}}) = \sqrt{2} \frac{1 + z}{\pi d_L(z)} \sqrt{\frac{dE}{df_s}}, \qquad (31)$$

where for the $\frac{dE}{df_s}$ we include the inspiral and merger phases, but ignore the contribution from the ringdown, which is short and characterized by a very fast reduction of the h_c with time (even in the high signal-to-noise GW150914 event).

In Fig. 7 (left panel), we show the evolution of the strain amplitude over frequency and time during the last second of the coalescence of two $30 \, M_\odot$ BHs following a circularized orbit. Assuming that the event occurs at a redshift of 0.09 and that the resulting final BH has a spin α of 0.67 (roughly corresponding to the best-fit values for the GW150914 event), we see that such an event would be easily traced over the expected final-design noise of LIGO [35], during a full second before the merger. If instead those black holes were on an elliptical orbit with eccentricity e evolving from 0.55 to 0.3 during that last second of the coalescence (right panel of Fig. 7), then GW power would be emitted also in other modes that at a given time are emitted from the source at frequencies $f_{n_{\text{source}}} = n \cdot f_{\text{orb}}$, where f_{orb} is the Keplerian orbital frequency of the binary. As can be clearly seen, in addition to observing the $n = 2$ (quadrupole) mode, LIGO with its expected final-design sensitivity should clearly be able to identify higher modes at least up to $n = 8$, since for frequencies > 50 Hz all these additional modes have a strain amplitude that is at least a factor of 3 higher than that of the noise. We discuss the details of how the strain amplitudes for those higher modes are calculated in the Appendix. We note that the extent to which the higher modes can be identified relies on the waveforms used by the LIGO collaboration. We also note that the eccentricity gets reduced within the last second of the inspiral, which changes the relative power of GWs between modes. As the eccentricity of the orbit is reduced, lower modes down to the quadrupole become more
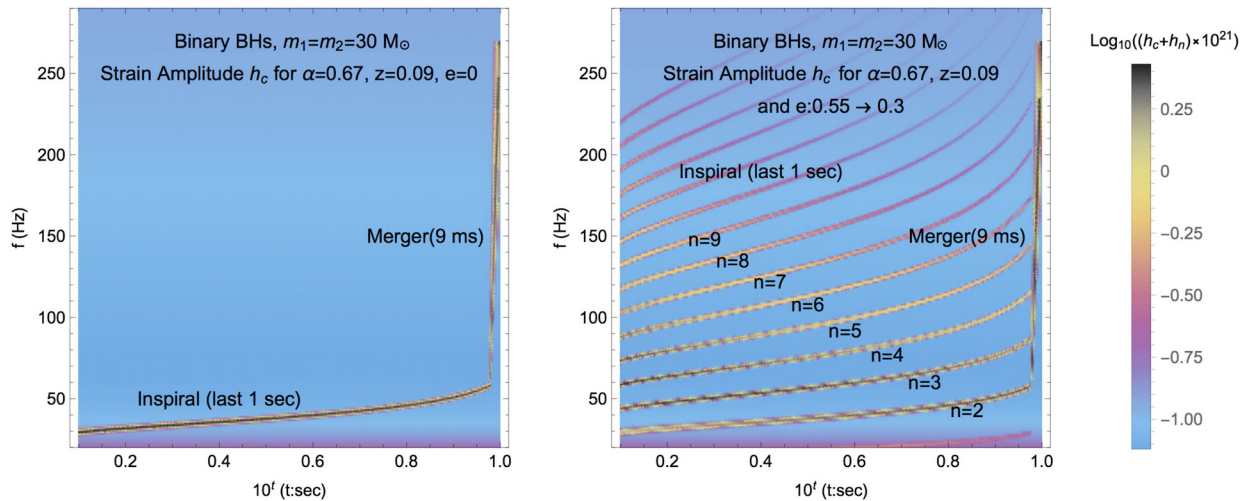

FIG. 7. Evolution over the last second of the amplitude of the signal strain, superimposed on the noise as expected with the LIGO design sensitivity. Time t here is between -1 and 0 seconds. Left: assuming no significant remaining eccentricity over that last one second. Right: assuming that during the last one second there is a remaining eccentricity that evolves from 0.55 to 0.3, resulting in the presence of higher GW modes than just the quadrupole ($n = 2$) one. The different mode amplitudes also evolve with time.
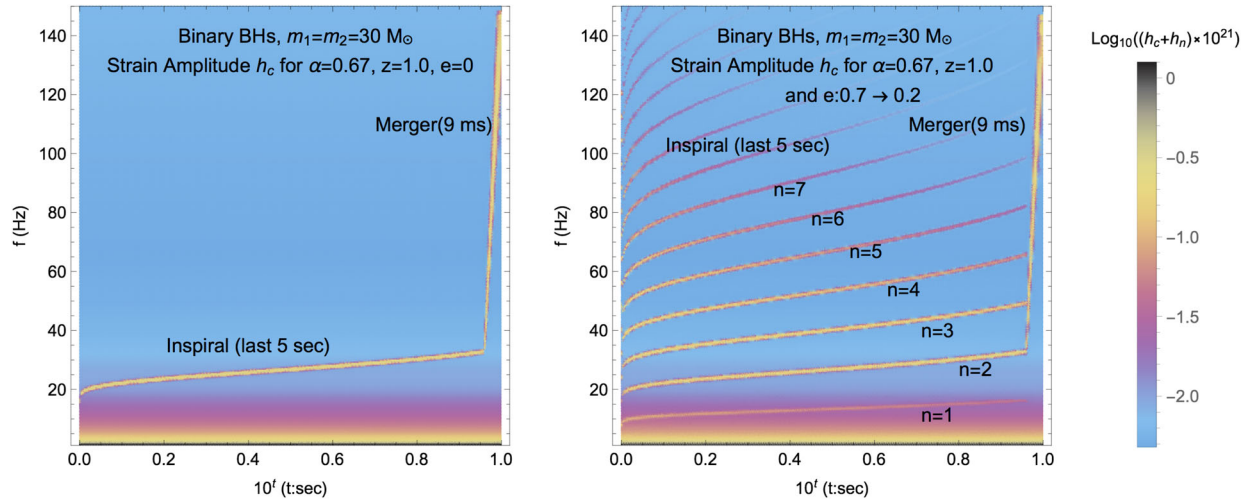
FIG. 8.   As in Fig. 7, assuming ET noise sensitivity instead. We plot the last 5 seconds. Left: assuming no significant remaining eccentricity over that last 5 seconds. Right: assuming that during the last 5 seconds there is an evolving eccentricity from 0.7 to 0.2. One can also see an $n = 1$ mode just above the background.

powerful over higher ones [40]. That should also be a matter of further investigation, to be accounted for by the waveform searches. That is because the rate of eccentricity evolution with time over the last phase of the inspiral depends on the exact realization of the BH binary coalescence.

With future detectors such as ET, the significantly lower noise and wider frequency range will allow us to follow coalescence events from further away and for a longer time. Figure 8 shows an equivalent merging event of two 30 $M_\odot$ BHs, but at a redshift of 1 and with an eccentricity of $e = 0$ ($e : 0.7 \to 0.2$), left (right), as that could be observed by ET. The first several higher modes could be followed for several seconds, possibly allowing even to probe the time evolution of the eccentricity of the individual coalescence events.

Observing higher modes can also allow the identification of events with eccentricity at the last stages of the inspiral with a higher signal-to-noise ratio (S/N) than that of the equivalent circularized objects. In fact, properly accounting for the presence of higher modes is relevant to

understanding the physical properties (mainly the masses and the distance) of the binary. In Table III, we present the expected S/N at LIGO and ET. For LIGO we assume the final-design sensitivity while for the Einstein Telescope we used the design option "ET-B" of Ref. [63], which is more pessimistic at low frequencies (relevant for high-mass BH coalescence events). As can be seen, the exact contribution to the S/N from the various GW modes at the inspiral depends on the eccentricity of the binary once its GWs enter the frequency band of the observatories, denoted here as e_{in} (not to be confused with the eccentricity at formation of the binary e_0), as well as the final e_{LSO}. Yet, for events with significant eccentricities during observation, higher modes can contribute significantly to the total S/N. Furthermore, these modes would reduce the overall contribution of the quadrupole mode to the S/N.

The results in Table III do not include the $n = 1$ mode since its contribution to the S/N is small and also depends on the exact assumptions of the instrument sensitivity at the lowest frequencies. For LIGO, the frequency band we

TABLE III.   The contribution of higher GW modes at elliptical orbits of 30 $M_\odot$ PBHs. We assume that when entering the frequency band of observation the binary has an initial eccentricity e_{in} that evolves down to e_{LSO}. The total S/N is the linear sum of columns 4–10 (we have accounted for the quadratic sum from the various phases). We take $\alpha = 0.67$ in Eq. (28) and $\epsilon = 0.04$ in Eq. (30). If we let $\alpha : (0.5$–$0.9)$ and $\epsilon : (0.03$–$0.05)$, there is a resulting 20% uncertainty in the values quoted in the fourth column.

Observatory Final design	z	$e_{in} \to e_{LSO}$	S/N Merger and ringdown	Δ(S/N) Inspiral ($n = 2$)	Δ(S/N) Inspiral ($n = 3$)	Δ(S/N) Inspiral ($n = 4$)	Δ(S/N) Inspiral ($n = 5$)	Δ(S/N) Inspiral ($6 \leq n \leq 10$)	Δ(S/N) Inspiral ($11 \leq n \leq 15$)
LIGO	0.09	$0 \to 0$	44	+25	...	...	...	...	...
LIGO	0.09	$0.6 \to 0$	44	+22	+33	+35	+31	+85	+19
LIGO	0.09	$0.6 \to 0.3$	44	+8.0	+30	+37	+33	+89	+19
LIGO	0.75	$0 \to 0$	6.8	+1.3	...	...	...	...	...
LIGO	0.75	$0.6 \to 0.3$	6.8	+1.2	+3.3	+4.2	+4.1	+11.8	+2.6
ET	1	$0 \to 0$	82	+16	...	...	...	...	...
ET	1	$0.6 \to 0.2$	82	+8.1	+35	+49	+50	+145	+32

assume starts as 20 Hz and for ET that frequency is 10 Hz. Any further advances that would allow those conservative values to be reduced would increase the S/N values quoted and the capacity of these observatories to identify elliptical orbits at coalescence.

The last orbits of the inspiral, the merger, and the ringdown have been the subject of numerical relativity and a variety of analytic approaches, where different orders of post-Newtonian approximation are implemented and where the impact of BH spins is included [64–70]. While future advances will certainly help in identifying GW events with higher modes, our quantitative results in this section should not be affected by these future developments. Such developments will affect predominantly the contributions of the merger and inspiral phases to the total S/N (fourth column in Table III). For the inspirals, more accurate waveforms in combination with lower instrumental noise will only affect how many of the higher modes will be identified and contribute to the S/N.

V. CONCLUSIONS

The possibility that the merger of primordial black holes may provide at least some of the gravitational-wave signals to be seen in the coming decade was first discussed in Ref. [3]. In this work, we investigated some of the implications of that hypothesis for future observations of gravitational waves.

We found that all binaries of PBHs, in all DM halos, are formed with high eccentricities. In the more massive halos, these binaries are characterized by small separations and short merger time scales, which can be as long as years and in some cases less than minutes. Consequently, some of the binaries retain a significant portion of their initial eccentricity as they enter the frequency bands of GW detectors. Even in the smallest halos we considered, $\sim 10^3 \, M_\odot$, there is a $O(1)\%$ chance that a merger will have a high eccentricity. Altogether, advanced LIGO is expected to observe $O(1)$ events with large eccentricities at the final stages of inspiral, while the ET should observe $O(10)$ such events.

These coalescences are characterized by detectably strong higher modes of GW waves. In fact, with ET we should be able to easily observe multiple higher modes from PBH binaries as far as redshifts $z \gtrsim 1$. The development of strategies to search for these higher modes is important, since misinterpretation of the physical properties (masses and redshift) of the coalescing binaries could result if they were missed. In addition, the total S/N can be significantly increased by measuring these higher modes.

We also considered eccentric events from competing astrophysical sources and found them likely to be a factor of 10 smaller, although uncertainties prevent a more definitive statement. We therefore conclude that a detection of highly eccentric 30 $M_\odot$ GW events will provide strong supporting evidence for the PBH progenitor scenario. Since

for some of the PBH binaries, the merger time scale is ∼years or less, with future observations at lower frequencies, such as those by eLISA [71], we may be able to follow such binaries through a longer era of their evolution (see for instance [72,73] for studies of stellar BH binaries). In fact, if proper waveforms are developed we may be able to detect GW emission from the formation event.

Strong evidence for a PBH-merger contribution to gravitational-wave events will likely require additional lines of evidence, including possibly some from cross-correlations of high-mass GW event locations with galaxy surveys [32], or an excess in the stochastic gravitational-wave background at lower frequencies (from higher redshifts, where the PBH should still reside) [74]. Furthermore, PBH binaries are formed from randomly moving BHs. We thus expect no correlation between the products $\vec{S}_1 \cdot \vec{L}$, $\vec{S}_2 \cdot \vec{L}$, where $\vec{S}_i$ is the spin of the individual BHs and $\vec{L}$ the angular momentum (note that this is a characteristic that is shared for all binaries formed through dynamical processes, rather than a common-envelope origin).

Ultimately, if the scenario considered here is correct, the mass distribution of an ensemble of events should demonstrate a significant contribution from high-mass BHs, and their measured properties, such as the eccentricity and spin, should be consistent with the two-body capture mechanism. In Ref. [3] we estimated that by the end of a six-year run at full sensitivity, LIGO should observe ∼600 PBH events. ET will observe roughly an order of magnitude more events. This should provide ample statistics to perform these tests.

APPENDIX: STRAIN AMPLITUDE FOR HIGHER MODES

Here we provide formulas needed to calculate the strain amplitude h_c used in Sec. IV C.

We define $f_{\mathrm{orb}}^{\min}$ at the minimal orbital frequency where there is contribution to GWs at detectable frequency ranges by a given experiment. GW modes are emitted at frequencies of

$$f_n = n \frac{f_{\mathrm{orb}}}{1+z} \quad \text{with} \quad n \geq 2. \tag{A1}$$

The current sensitivity of LIGO has a minimum of $f^{\min} = 20$ Hz with the design sensitivity being $f^{\min} = 10$ Hz, and

with the future ET expected design sensitivity being at $f^{\min} = 2$ Hz. Thus the relevant $f^{\min}_{\rm orb}$ are 10, 5 and 1 Hz, respectively. In this work we use $f^{\min}_{\rm orb} = 10$ Hz for LIGO and 5 Hz for ET as a conservative estimate. Thus, for a given eccentricity, LIGO or ET observe the inspiraling binary when its pericenter is at most

$$r^{\rm in}_{\rm per}(m_1, m_2, e) = \left(\frac{2\pi}{f^{\min}_{\rm orb}} (1 + e^{\rm in})^{1/2} G^{1/2} m^{1/2}_{\rm tot} \right)^{\frac{2}{3}}, \quad \text{(A2)}$$

or in its dimensionless form at

$$\rho(m_1, m_2, e^{\rm in}) = \frac{r^{\rm in}_{\rm per}(m_1, m_2, e^{\rm in}) G^{-1} c^2}{m_{\rm tot}}. \quad \text{(A3)}$$

The spectral energy densities of higher modes at a given eccentricity can be evaluated based on the quadrupole mode at the same time by [40]

$$\frac{dE^{n \geq 2}}{df_{s\,{\rm inspiral}}} = \frac{2}{n} \frac{g(n, e)}{g(2, e)} \frac{dE^{n=2}}{df_{s\,{\rm inspiral}}}, \quad \text{(A4)}$$

where

$$g(n, e) = \frac{n^4}{32} \left[\left(J_{n-2} - 2eJ_{n-1} + \frac{2}{n} J_n + 2eJ_{n+1} - J_{n+2} \right)^2 \right.$$
$$\left. + (1 - e^2)(J_{n-2} - 2J_n + J_{n+2})^2 + \frac{4}{3n^2} J_n^2 \right], \quad \text{(A5)}$$

and J_n is the Bessel function of order n evaluated at ne. For $n = 1$ we use that [40]

$$\sum_{n=1}^{n=\infty} = \frac{1 + \frac{73}{24} e^2 + \frac{37}{96} e^4}{(1 - e^2)^{7/2}}. \quad \text{(A6)}$$

For the total signal-to-noise ratio we used [39]

$$\langle S^2/N^2 \rangle_{\rm inspiral} = 2 \frac{48}{95} \frac{\eta(m_{\rm tot}(1+z))^3 \rho(m_1, m_2, e^{\rm in})}{dL^2(z)}$$
$$\times \sum_{n=1}^{n_{\max}} \int_{f^{\min}}^{f^{\max}} \frac{df}{f} \frac{n g(n, e) s(e, e_{\rm in})}{e(1+z) f S_n(f)} \quad \text{(A7)}$$

and

$$\langle S^2/N^2 \rangle_{\rm merger+ringdown} = 2 \frac{4}{5} \int_{f^{\min}}^{f^{\max}} df \frac{h_c^2(f)}{S_n(f)(2f)^2} \quad \text{(A8)}$$

with

$$s(e, e_{\rm in}) = \left(\frac{e}{e_{\rm in}} \right)^{\frac{24}{19}} \left(\frac{1 + \frac{121}{304} e^2}{1 + \frac{121}{304} e_{\rm in}^2} \right)^{\frac{1740}{2299}}$$
$$\times \left(\frac{(1 + e_{\rm in}^2)(1 - e^2)^{3/2}}{1 - \frac{183}{304} e^2 - \frac{121}{304} e^4} \right). \quad \text{(A9)}$$

In Eqs. (A7) and (A8), $S_n(f)$ is the strain noise amplitude $(h_n(f))$ squared; f is $f_{\rm obs}$.

---

[1] B. P. Abbott *et al.* (Virgo and LIGO Scientific Collaboration), Phys. Rev. Lett. **116,** 061102 (2016).

[2] B. P. Abbott *et al.* (Virgo and LIGO Scientific Collaboration), Phys. Rev. Lett. **116,** 241103 (2016).

[3] S. Bird, I. Cholis, J. B. Muñoz, Y. Ali-Haïmoud, M. Kamionkowski, E. D. Kovetz, A. Raccanelli, and A. G. Riess, Phys. Rev. Lett. **116,** 201301 (2016).

[4] T. Hosokawa, S. Hirano, R. Kuiper, H. W. Yorke, K. Omukai, and N. Yoshida, Astrophys. J. **824,** 119 (2016).

[5] C. L. Rodriguez, S. Chatterjee, and F. A. Rasio, Phys. Rev. D **93,** 084029 (2016).

[6] B. Zhang, Astrophys. J. **827,** L31 (2016).

[7] S. E. Woosley, Astrophys. J. **824,** L10 (2016).

[8] S. Chatterjee, C. L. Rodriguez, and F. A. Rasio, arXiv:1603.00884.

[9] S. E. de Mink and I. Mandel, Mon. Not. R. Astron. Soc. **460,** 3545 (2016).

[10] T. Hartwig, M. Volonteri, V. Bromm, R. S. Klessen, E. Barausse, M. Magg, and A. Stacy, Mon. Not. R. Astron. Soc. **460,** L74 (2016).

[11] K. Inayoshi, K. Kashiyama, E. Visbal, and Z. Haiman, arXiv:1603.06921.

[12] A. Arvanitaki, M. Baryakhtar, S. Dimopoulos, S. Dubovsky, and R. Lasenby, arXiv:1604.03958.

[13] C. L. Rodriguez, C.-J. Haster, S. Chatterjee, V. Kalogera, and F. A. Rasio, Astrophys. J. **824,** L8 (2016).

[14] T. L. S. Collaboration and T. V. Collaboration (The Virgo, The LIGO Scientific), arXiv:1606.04856.

[15] B. P. Abbott *et al.* (Virgo and LIGO Scientific Collaboration), arXiv:1602.03842.

[16] B. P. Abbott *et al.* (Virgo and LIGO Scientific Collaboration), Phys. Rev. Lett. **116,** 241102 (2016).

[17] B. J. Carr, Astrophys. J. **201,** 1 (1975).

[18] B. J. Carr and S. W. Hawking, Mon. Not. R. Astron. Soc. **168,** 399 (1974).

[19] P. Meszaros, Astron. Astrophys. **37,** 225 (1974).

[20] B. J. Carr, K. Kohri, Y. Sendouda, and J. Yokoyama, Phys. Rev. D **81,** 104019 (2010).

[21] M. A. Monroy-Rodríguez and C. Allen, Astrophys. J. **790,** 159 (2014).

[22] R. A. Allsman *et al.* (Macho Collaboration), Astrophys. J. **550,** L169 (2001).

[23] P. Tisserand *et al.* (EROS-2 Collaboration), Astron. Astrophys. **469,** 387 (2007).

[24] L. Wyrzykowski *et al.*, Mon. Not. R. Astron. Soc. **416,** 2949 (2011).

[25] D. Pooley, S. Rappaport, J. Blackburne, P. L. Schechter, J. Schwab, and J. Wambsganss, Astrophys. J. **697,** 1892 (2009).

[26] E. Mediavilla, J. A. Munoz, E. Falco, V. Motta, E. Guerras, H. Canovas, C. Jean, A. Oscoz, and A. M. Mosquera, Astrophys. J. **706,** 1451 (2009).

[27] E. Bugaev and P. Klimai, Phys. Rev. D **83,** 083521 (2011).

[28] J. Yoo, J. Chaname, and A. Gould, Astrophys. J. **601,** 311 (2004).

[29] D. P. Quinn, M. I. Wilkinson, M. J. Irwin, J. Marshall, A. Koch, and V. Belokurov, Mon. Not. R. Astron. Soc. **396,** L11 (2009).

[30] M. Ricotti, J. P. Ostriker, and K. J. Mack, Astrophys. J. **680,** 829 (2008).

[31] T. D. Brandt, Astrophys. J. **824,** L31 (2016).

[32] A. Raccanelli, E. D. Kovetz, S. Bird, I. Cholis, and J. B. Munoz, Phys. Rev. D **94,** 023516 (2016).

[33] T. Namikawa, A. Nishizawa, and A. Taruya, Phys. Rev. D **94,** 024013 (2016).

[34] J. B. Muñoz, E. D. Kovetz, L. Dai, and M. Kamionkowski, Phys. Rev. Lett. **117,** 091301 (2016).

[35] J. Aasi *et al.* (Virgo and LIGO Scientific Collaboration), Living Rev. Relativ. **19,** 1 (2016).

[36] B. Sathyaprakash *et al.*, in *2011 Gravitational Waves and Experimental Gravity*, edited by E. Auge, J. Dumarchez, and J. T. Thanh Van (The Gioi Publishers, Vietnam, 2011).

[37] S. Clesse and J. García-Bellido, arXiv:1603.05234.

[38] M. Sasaki, T. Suyama, T. Tanaka, and S. Yokoyama, Phys. Rev. Lett. **117,** 061101 (2016).

[39] R. M. O'Leary, B. Kocsis, and A. Loeb, Mon. Not. R. Astron. Soc. **395,** 2127 (2009).

[40] P. C. Peters and J. Mathews, Phys. Rev. **131,** 435 (1963).

[41] M. Turner, Astrophys. J. **216,** 610 (1977).

[42] P. C. Peters, Phys. Rev. **136,** B1224 (1964).

[43] S. F. Kulkarni, S. McMillan, and P. Hut, Nature (London) **364,** 421 (1993).

[44] V. Kalogera, A. King, and F. A. Rasio, Astrophys. J. **601,** L171 (2004).

[45] V. Kalogera, K. Belczynski, C. Kim, R. W. O'Shaughnessy, and B. Willems, Phys. Rep. **442,** 75 (2007).

[46] D. Vanbeveren, New Astron. Rev. **53,** 27 (2009).

[47] M. Dominik, K. Belczynski, C. Fryer, D. E. Holz, E. Berti, T. Bulik, I. Mandel, and R. O'Shaughnessy, Astrophys. J. **779,** 72 (2013).

[48] N. Mennekens and D. Vanbeveren, Astron. Astrophys. **564,** A134 (2014).

[49] M. Dominik, E. Berti, R. O'Shaughnessy, I. Mandel, K. Belczynski, C. Fryer, D. Holz, T. Bulik, and F. Pannarale, Astrophys. J. **806,** 263 (2015).

[50] I. Mandel and S. E. de Mink, Mon. Not. R. Astron. Soc. **458,** 2634 (2016).

[51] A. I. Bogomazov, V. M. Lipunov, and A. V. Tutukov, Astronomy Reports **51,** 308 (2007).

[52] M. Holman, J. Touma, and S. Tremaine, Nature (London) **386,** 254 (1997).

[53] F. Antonini, S. Chatterjee, C. L. Rodriguez, M. Morscher, B. Pattabiraman, V. Kalogera, and F. A. Rasio, Astrophys. J. **816,** 65 (2016).

[54] A. D. Ludlow, S. Bose, R. E. Angulo, L. Wang, W. A. Hellwing, J. F. Navarro, S. Cole, and C. S. Frenk, Mon. Not. R. Astron. Soc. **460,** 1214 (2016).

[55] F. Prada, A. A. Klypin, A. J. Cuesta, J. E. Betancort-Rijo, and J. Primack, Mon. Not. R. Astron. Soc. **423,** 3018 (2012).

[56] M. Morscher, S. Umbreit, W. M. Farr, and F. A. Rasio, Astrophys. J. **763,** L15 (2013).

[57] I. Harry, S. Privitera, A. Bohé, and A. Buonanno, Phys. Rev. D **94,** 024012 (2016).

[58] F. Antonini, N. Murray, and S. Mikkola, Astrophys. J. **781,** 45 (2014).

[59] W. E. Harris, Astron. J. **112,** 1487 (1996).

[60] P. Kroupa, Mon. Not. R. Astron. Soc. **322,** 231 (2001).

[61] C. L. Rodriguez, M. Morscher, B. Pattabiraman, S. Chatterjee, C.-J. Haster, and F. A. Rasio, Phys. Rev. Lett. **115,** 051101 (2015); **116,** 029901(E) (2016).

[62] E. E. Flanagan and S. A. Hughes, Phys. Rev. D **57,** 4535 (1998).

[63] B. Sathyaprakash *et al.*, Classical Quantum Gravity **29,** 124013 (2012); **30,** 079501(E) (2013).

[64] A. Buonanno, Y.-b. Chen, and M. Vallisneri, Phys. Rev. D **67,** 104025 (2003); **74,** 029904(E) (2006).

[65] L. Blanchet, T. Damour, G. Esposito-Farese, and B. R. Iyer, Phys. Rev. Lett. **93,** 091101 (2004).

[66] L. Blanchet, A. Buonanno, and G. Faye, Phys. Rev. D **74,** 104034 (2006); **81,** 089901(E) (2010).

[67] L. Blanchet, G. Faye, B. R. Iyer, and S. Sinha, Classical Quantum Gravity **25,** 165003 (2008); **29,** 239501 (2012).

[68] K. G. Arun, A. Buonanno, G. Faye, and E. Ochsner, Phys. Rev. D **79,** 104023 (2009); **84,** 049901(E) (2011).

[69] P. Ajith *et al.*, Phys. Rev. Lett. **106,** 241101 (2011).

[70] P. Ajith, Phys. Rev. D **84,** 084037 (2011).

[71] P. Amaro-Seoane *et al.*, Classical Quantum Gravity **29,** 124016 (2012).

[72] A. Nishizawa, E. Berti, A. Klein, and A. Sesana, Phys. Rev. D **94,** 064020 (2016).

[73] A. Nishizawa, A. Sesana, E. Berti, and A. Klein, arXiv:1606.09295.

[74] V. Mandic, S. Bird, and I. Cholis, arXiv:1608.06699.